IET Renewable Power Generation

An Auxiliary Dead-Band Controller for the Coordination of Fast Frequency Support from Multi-Terminal HVDC Grids and Offshore Wind Farms

RPG-2018-5485 | Research Article

Submitted by: Khadijat Jose, Tibin Joseph, Jun Liang, Carlos Ernesto Ugalde-Loo

Keywords: FREQUENCY RESPONSE, FREQUENCY CONTROL, FREQUENCY STABILITY, HVDC, OFFSHORE WINDFARM, VOLTAGE-SOURCED CONVERTER (VSC)

An Auxiliary Dead-Band Controller for the Coordination of Fast Frequency Support from Multi-Terminal HVDC Grids and Offshore Wind Farms

Khadijat Jose [1*], Tibin Joseph[1], Jun Liang[1], Carlos E. Ugalde-Loo[1]

[1] School of Engineering, Cardiff University, Queen's Buildings, The Parade, Cardiff, CF24 3AA, Wales, UK
[*]JoseK2@cardiff.ac.uk

Abstract: High-voltage direct-current (HVDC) grids may provide fast frequency support to ac grids with the aid of supplementary control algorithms and synthetic inertia contribution from offshore wind farms. However, when all converters within the HVDC grid are fitted with these supplementary controllers, undesirable power flows and reduced power transfers may occur during a power imbalance. This is due to simultaneous frequency oscillations on the different ac systems connected to the HVDC grid arising during the support operation. To prevent this adverse effect, an auxiliary dead-band controller (ADC) is proposed in this paper. The ADC modifies the dead-band set-point of the fast frequency controllers using measurements of rate of change of frequency and frequency deviation. A four-terminal HVDC integrated with an offshore wind farm is modelled to analyse and study the effectiveness of three different supplementary fast frequency control algorithms. Results show that the proposed ADC scheme improves the performance of fast frequency control algorithms. For completeness, a small-signal stability analysis is carried out to confirm that a stable system operation is maintained.

1. Introduction

Offshore wind generation will provide a major share of the world's future energy generation mix. It is expected that the total offshore wind capacity in Europe will be 23 GW by 2020 and it is projected to rise to 66 GW by 2030 [1]. Power generated from this renewable source will be mainly transmitted using high-voltage direct-current (HVDC) systems. In Great Britain the wind resource is very high and it is expected that 9 GW of HVDC interconnection and 22 GW of offshore wind capacity will replace 13 GW of conventional generation capacity by 2020 [2].

HVDC converters, wind turbines (WTs) and other power electronics based low carbon generators do not contribute to the system inertia. Therefore, changes in the generation mix of power systems with a high penetration of renewables will lead to a major reduction in the total inertia [3]. This reduction translates into higher frequency deviations and a faster rate of change of frequency (*RoCoF*) when the grid experiences a disturbance [3].

Given the projected changes in the power generation mix, it is important to ensure the stability and security of the power system. For this, the transmission system operators set Grid Codes. For instance, the European Network of Transmission System Operators for Electricity (ENTSO-E) requires voltage source converters (VSCs) to provide ancillary services to the interconnected ac grids. Some of these services include fault-ride through and fast frequency support from multi-terminal HVDC (MTDC) grids [4], [5].

Conventional synchronous generators automatically respond to system imbalance by releasing kinetic energy stored in their rotating shafts to maintain equilibrium between generation and demand. The amount of kinetic energy released is proportional to the inertia of the rotating machine [6]. However, HVDC-connected offshore wind farms (OWFs) do not behave this way. If variable-speed WTs are employed, their power electronics based grid side converter (GSC) decouples the generator's frequency from the grid's frequency and therefore, an imbalance in the power system cannot be detected [7]. To address this, synthetic inertia schemes from OWFs and coordination of fast frequency support from ac systems connected to VSC-HVDC systems have been proposed [8]. In WTs, synthetic inertia is possible using supplementary control loops which release stored kinetic energy in the turbine to support the system frequency during an imbalance [9].

Several supplementary control schemes for the coordination of fast frequency support from VSC-MTDC have been proposed in the open literature. They aim to provide quick power transfer from OWFs or from other ac systems connected to the dc grid and the VSC capacitors. In general, the supplementary schemes can be classified as either communication-based or communications-free. Communication-based frequency support control uses communication channels such as optical fibre and SCADA [10], [11] to transmit frequency measurements between the different converter stations in the dc grid [11], [12]. These methods use the frequency deviation or the frequency derivative to modulate active power from the wind farms or other onshore grids as in [13].

Communications-free schemes use local signals, such as dc voltage, to reflect the changes in the ac grid frequency. With these methods, response times during frequency support are minimised and potential issues arising from long distance transmission are eliminated [14]. In addition, the need for a large investment in communication links is removed, together with risks associated to communication delays and signal interruptions [15]. Moreover, it has been shown in [11] that communication-free schemes can achieve a quite similar frequency support performance as communication-based methods. Due to these attributes, the scope of this work is restricted to communication-free frequency support schemes. Among these, the main schemes are based on proportional droop controllers: frequency-active-power (*f-P)* droop, frequency-dc-link-voltage (f-V_{dc}) droop and dual loop (which

combines frequency vs dc-voltage vs active power (f-V_{dc}-P) characteristics) [5], [7], [16].

A derivative based supplementary control has been also proposed in the literature; however, it does not provide as much support as the proportional droop control methods [17], [18]. Although these schemes have been tested and shown to be effective on MTDC grids, it has been assumed that not every ac system connected to the MTDC grid requires frequency support. Thus, only the onshore VSCs connected to the ac system requiring the fast frequency support service have been fitted with the auxiliary loops [5], [7], [16]. If all the onshore VSCs are upgraded with the supplementary controllers, those converters connected to the main ac grid experiencing a disturbance would be the first to activate their frequency sensitive mode. However, the other ac grids may begin to experience a drop in frequency when they provide support in response to the disturbance and, in turn, this would activate the frequency sensitive mode of those VSCs connected to them. This would ultimately cause their dc voltage droop control to deactivate. Such operation could result in undesirable power flows and reduced power transfers through the MTDC grid, limiting the overall ability to provide frequency support due to potential adverse interactions between the different VSC supplementary control schemes [16].

To address the aforementioned shortcoming, the operation of an MTDC system upgraded with the main fast frequency control schemes reported in literature is investigated. All onshore VSCs are fitted with the supplementary controllers. An auxiliary dead-band control (ADC) scheme is proposed to work alongside the fast frequency control algorithms. As it will be observed, the ADC scheme improves the frequency support capability of the conventional methods and ensures system stability during multiple ac system frequency oscillations. To demonstrate the performance of the proposed ADC scheme, a four-terminal VSC-HVDC system with one OWF connected to three separate ac systems is modelled in MATLAB/Simulink. The OWF is suitably controlled to provide frequency support via synthetic inertia during these studies. Given that the penetration of power electronics connected renewable sources is increasing and if supplementary controllers and synthetic inertia are added, it is important to investigate their impact on system stability. Therefore, the effects of these fast frequency support schemes and of the ADC on the entire power system operation was investigated using small-signal stability analysis.

This paper builds on the initial results presented in [19]. The inertial contribution of OWF is considered here in coordination with the frequency support and it changes the system behaviour. The main contributions of the paper are: (1) the coordination of fast frequency algorithms in MTDC grids and synthetic inertia from OWFs under single and multiple imbalances; (2) the stability of the system is quantified to demonstrate an improved system operation during imbalances when supplementary frequency controllers are fitted to all converters in the dc grid; (3) a small-signal stability study of the MTDC system (including the OWF and ac grids) is carried out to demonstrate system stability.

2. Control of DC Grid Converters

Onshore converter control in an MTDC grid ensures a correct power balance among converters. The architecture consists of a cascaded control loop structure based on dq transformations to achieve an independent control of active and reactive power. A fast-inner control loop regulates the d and q-axis currents. DC voltage, power, ac voltage and reactive power are controlled with outer loops [4], [20]. To this end, constant power, constant dc voltage or dc voltage-active power droop control can be used.

Droop control is employed in this paper for dc voltage (V_{dc}) and power (P) control. The onshore GSCs employ V_{dc}-P control on the d-axis and reactive power (Q) or ac voltage (V) control on the q-axis. A power- dc voltage droop creates a proportional relationship between voltage and power. Since dc voltage control in a dc grid is analogous to frequency control in ac grids, the dc voltage will change in response to variations in dc current. This change in dc voltage can be used as an indicator for converters to share the power imbalance. Droop control also allows for redundancy in comparison to master-slave control [17]. In a master-slave control scheme, a single converter regulates the dc voltage of the MTDC grid. If this slack converter is lost, then the operation of the dc grid will be compromised. However, the responsibility of controlling the dc voltage can be distributed over a number of converters if droop control is employed. Thus, losing one converter will not lead to the outage of the dc grid [21].

The offshore wind farm converter (WFC) creates an ac voltage with fixed magnitude, frequency and phase angle. The WFCs gather all the power generated from OWFs and transfer it into the dc grid [20]. Fig. 1(a) shows the control structures in a three-terminal scheme, with onshore VSCs 1 and 2 operating in V_{dc}-P droop.

3. Wind Turbines Temporary Overproduction

In this paper, the OWF is made of 150 aggregated fully rated converter WT units of 5 MVA each based on permanent magnet synchronous generators (PMSGs). The OWF has a total rated capacity of 750 MVA. It is assumed that the OWF operates at wind speed of 10.5 m/s and maximum power point tracking (MPPT) is used to regulate the rotational speed of the generator to obtain the maximum power.

Fig. 1(b) shows the PMSG-WT control scheme. The rotor side converter (RSC) regulates the torque (or power) from the PMSG while the network side converter (NSC) regulates the dc voltage. More information on the detailed modelling of the PMSG-WT can be found in [22]. The OWF also contributes to support the frequency of the ac systems by inertia emulation. Inertial contribution from WTs for frequency support is well discussed in the literature [12], [23], [24].

Temporary overproduction is the inertia emulation strategy considered in this paper and it is shown in Fig. 1(c). It involves a temporary step increase in the power/torque generated from the WT [23], [24], [19]. When the WTs detect a decline in system frequency, they reduce their speed to release 5-10% extra power from the stored kinetic energy in their rotating shafts. This temporary overproduction of power is held for some seconds and then the WT speed begins to increase to resume its original operating condition.

For frequency support provision, the offshore WFC must be fitted with a supplementary dc voltage-frequency (V_{dc}-f) droop controller [7], [12]. This varies the frequency of the offshore ac system based on changes to the dc voltage according to

$$f_{off} = f_{off,0} - k_{off}(V_{dc,0} - V_{dc}) \quad (1)$$

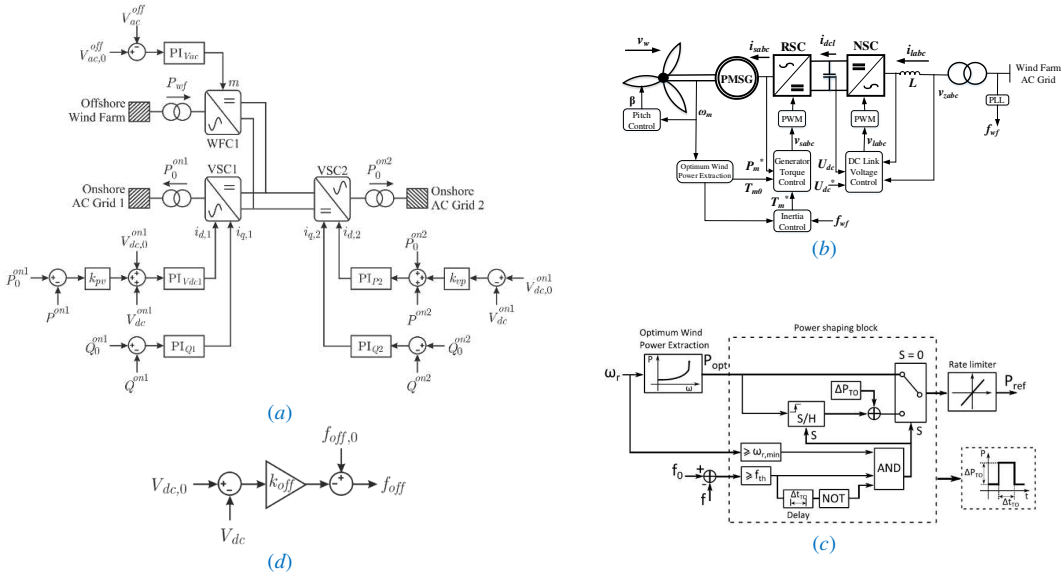

Figure 1: *Frequency support from OWFs. (a) Outer-loop controllers of VSCs showing droop control (inner current loops not shown) (b) PMSG-WT control scheme. (c) WT temporary overproduction scheme* [25]. *(d) Droop control of WFC for fast frequency support*

where k_{off} is the dc voltage-frequency droop gain, f_{off} is the offshore ac grid frequency, and $f_{off,0}$ is the reference frequency. The V_{dc}-f droop scheme is shown in Fig. 1(d)

4. MTDC Fast Frequency Support Schemes

In this section, the frequency control schemes are classified as switching and non-switching based schemes. In the switching-based schemes, there is a switch between one droop to the other. Conversely, droops are used together or communications are employed for frequency control in the non-switching based schemes.

4.1. Switching-based Frequency Control Schemes

4.1.1 Coordinated Control Scheme: Shown in Fig. 2(a), the coordinated control (CC) scheme uses a P-V_{dc} droop during normal operation ($f_{on,0} - f_{on} < \Delta f_{db}$) but then switches to a supplementary f-V_{dc} droop following a frequency disturbance ($f_{on,0} - f_{on} \geq \Delta f_{db}$) [5]. This can be expressed as follows:

$$\begin{cases} V_{dc}^{*} = V_{dc,0} - k_{pv}(P_{dc,0} - P_{dc}), & \text{if } (f_{on,0} - f_{on}) < \Delta f_{db} \\ V_{dc}^{*} = V_{dc,0} + k_{fv}(f_{on,0} - f_{on}), & \text{if } (f_{on,0} - f_{on}) \geq \Delta f_{db} \end{cases} \quad (2)$$

where k_{pv} is the active power-dc voltage droop gain and k_{fv} is the frequency-dc voltage droop gain. The f-V_{dc} droop transforms the ac frequency deviation into a proportional dc voltage signal which, in turn, modifies the reference value of the dc voltage at the VSC terminal. After recovery from the disturbance, the system will return to the original P-V_{dc} droop when $(f_{on,0} - f_{on}) < \Delta f_{db}$, where Δf_{db} is the dead-band set-point of the frequency support loop. To prevent adverse transients from occurring, a sample and hold block is used to hold the pre-disturbance value of the dc voltage when switching to f-V_{dc} droop occurs [5].

4.1.2* Alternative Coordinated Control Scheme:* Shown in Fig. 2(b), the alternative coordinated control (ACC) scheme uses a V_{dc}-P droop during normal operation and switches to an f-P droop during a disturbance [7]. This can be expressed as:

$$\begin{cases} P_{dc}^{*} = P_{dc,0} - k_{vp}(V_{dc,0} - V_{dc}), & \text{if } (f_{on,0} - f_{on}) < \Delta f_{db} \\ P_{dc}^{*} = P_{dc,0} + k_{fp}(f_{on,0} - f_{on}), & \text{if } (f_{on,0} - f_{on}) \geq \Delta f_{db} \end{cases} \quad (3)$$

with

$$k_{fp} = \frac{k_{fv}}{k_{pv}}, \; k_{vp} = \frac{1}{k_{pv}},$$

where k_{vp} is the dc voltage-active power droop gain (defined as the inverse of k_{vp} for an active power-dc droop gain, see CC scheme) and k_{fp} is the frequency-active power droop gain (defined in terms of the droop gains of the CC scheme). After the disturbance event is over, the system will return to the original V_{dc}-P droop when $(f_{on,0} - f_{on}) < \Delta f_{db}$. A sample and hold block is employed to hold the pre-disturbance value of the active power when switching to the f-P droop occurs.

It should be highlighted that the ACC scheme enables the TSO to have direct control of the required power to be delivered by a converter by adjusting the droop gain k_{fp}. However, the droop gains k_{fv} and k_{pv} would need to be modified for a CC scheme so that an equivalent amount of power delivery is achieved.

4.2 Non-Switching Frequency Control Schemes

4.2.1 Dual-loop Control Scheme: The dual-loop control (DLC) scheme is similar to the CC scheme. However, it combines the frequency and voltage droop control techniques unlike the CC scheme, where the P-V_{dc} droop is deactivated when the f-V_{dc} droop is in use. It is shown in Fig. 2(c). The DLC scheme is mathematically expressed below:

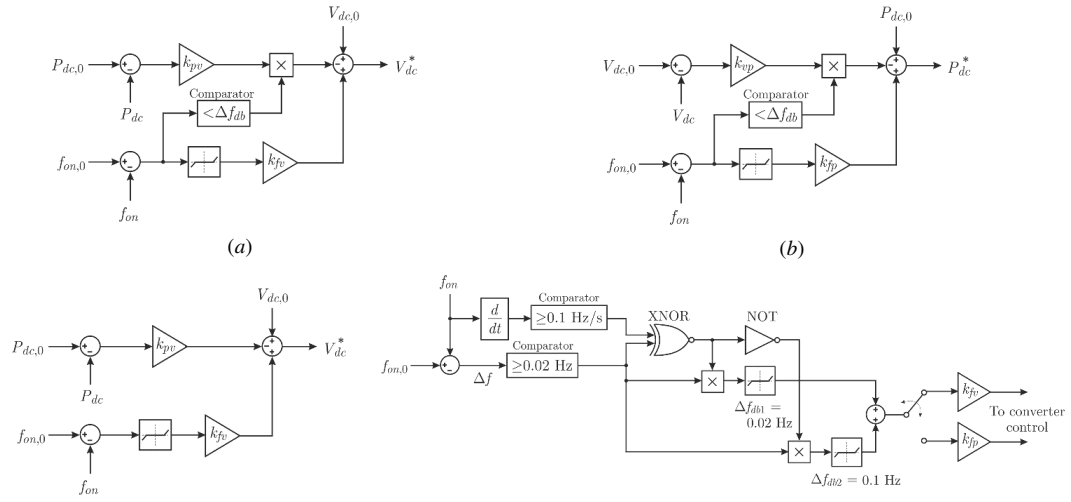

Figure 2: *Fast frequency control schemes: (a) CC; (b) ACC; (c) DLC; (d) proposed ADC. Comparators output either 0 or 1.*

$$\begin{cases} V_{dc}^* = V_{dc,0} - k_{pv}(P_{dc,0} - P_{dc}), \text{ if } (f_{on,0} - f_{on}) < \Delta f_{db} \\ V_{dc}^* = V_{dc,0} - k_{pv}(P_{dc,0} - P_{dc}) + k_{fv}(f_{on,0} - f_{on}), \\ \qquad\qquad \text{if } (f_{on,0} - f_{on}) \geq \Delta f_{db} \end{cases} \quad (4)$$

During normal operation, the P-V_{dc} droop is in operation and when a frequency disturbance is detected (*i.e.* $f_{on,0} - f_{on} < \Delta f_{db}$, the f-V_{dc} droop is activated and works simultaneously with the P-V_{dc} droop [16]. Therefore, there is no switching between the droops.

4.2.2 Weighted Frequency Scheme*:* This scheme was originally proposed as an alternative to the CC scheme. It requires fast communications of onshore frequency variations to the offshore converters. A weighted sum of the onshore ac frequency deviations is calculated, which is in turn used to control the OWF frequency [9].

4.2.3 Other frequency control schemes: Reference [12] proposes the use of joint f-P and V_{dc}-P droop controllers in the onshore converters without the use of a dead-band.

Communications-based schemes are out of the scope of this paper and hence are not discussed.

4.3 Drawback of Fast Frequency Control Schemes

When an ac system connected to an MTDC grid experiences a power disturbance, other ac grids connected to the dc grid will respond to provide support to the disturbed grid if droop control is used. While providing support, the responding grids will experience frequency variations which could exceed the dead-band set on their VSC terminal and, in turn, activate the fast frequency support schemes of the VSCs connected to them (if fitted with supplementary controllers). As a result, their voltage-power droop would be automatically disabled. Under this circumstance, no VSC in the MTDC grid will regulate the dc voltage and instability may arise. Thus, it is important to coordinate the dead-band set-point of the frequency control algorithms fitted to the different converters so that stable power flows and power transfer capability can be restored during multiple ac frequency variations.

It should be borne in mind that a future MTDC grid may encompass different control methodologies –including those presented in this paper. It would be possible that the described drawback is not applicable if a converter within the dc grid is always controlling dc voltage. However, the presence of a dc voltage controlling converter on its own would undermine the distributed control principle of droop control [10].

5 Auxiliary Dead-Band Controller

To coordinate the provision of fast frequency support in an MTDC grid and to eliminate the aforementioned drawbacks, an ADC is proposed. This is shown in Fig. 2(d). It discriminates between those VSCs connected to disturbed ac grids from those connected to responding ac grids during fast frequency support.

The ADC is connected at each converter station and is used in conjunction with the converter's supplementary frequency controller discussed in Section 4. The ADC operates as follows: it uses the local frequency measurement of the ac grid it is connected to and uses this measurement to calculate frequency deviation Δf and the *RoCoF*. The value of Δf is passed through a comparator block and if it is greater than a threshold value of 0.02 Hz, an output of 1 is produced (otherwise the output is 0). The frequency deviation threshold of 0.02 Hz is selected as established by ENTSO-E [26]. Similarly, the *RoCoF* measurement is compared to a threshold of 0.1 Hz/s. If its value is greater than the threshold, an output of 1 is produced (otherwise an output of 0 is obtained). It should be highlighted that the *RoCoF* threshold value of 0.1 Hz/s is less than the current set-point of 0.25 Hz/s, which is employed to trigger protection devices [27], [28].

The outputs from the Δf *and RoCoF* comparators are then sent to an XNOR gate, which produces a true (1) output when all its inputs are either false (0) or true (1). Its logic is shown in Table 1. This way, the XNOR gate can produce an output which enables the modification of the dead-band set-point of the supplementary frequency controllers. For instance, when the XNOR output is 0, the dead-band set-point will be 0.1 Hz; conversely, when it is 1, the dead-band will be set to 0.02 Hz.

During normal ac grid operation, the ADC allows all the supplementary controllers dead-band set-points to be 0.02 Hz. This occurs as their Δf and *RoCoF* are less than 0.02 Hz and 0.1 Hz/s; thus, the XNOR gate produces a true (1) output. During a frequency disturbance, the *RoCoF* and Δf begin to change. If their values exceed 0.02 Hz and 0.1 Hz/s, respectively, a true output (1) is still produced on both comparators (see Fig. 2(d)), which leads to a true (1) output from the XNOR gate (see Table 1). This implies that a dead-band value of $\Delta f_{db1} = 0.02$ Hz is kept. For converters connected to the responding grids, Δf may become higher than 0.02 Hz due to the active power they are transferring to the disturbed grid for frequency support; however, their measured *RoCoF* may be less than 0.1 Hz/s. Under these circumstances, an XNOR output of 0 is produced, which the NOT gate inverts to 1. This in turn changes the dead-band from $\Delta f_{db1} = 0.02$ Hz to $\Delta f_{db2} = 0.1$ Hz in the responding converters.

It is important to note that the ADC only uses the local frequency measurement of its own grid. The ADC will allow for stable operation of the dc grid during fast frequency support and prevents the need for communications in determining which grid requires support.

Table 1: *ADC XNOR Logic.*

RoCoF (Hz/s)	Δf (Hz)	XNOR gate	Dead-band value (Hz)
≥0.1	≥0.02	1	0.02
≥0.1	≤0.02	0	0.1
≤0.1	≥0.02	0	0.1
≤0.1	≤0.02	1	0.02

6 Simulations and Results

The four-terminal VSC-HVDC test system shown in Fig. 3 is used to compare the effectiveness of the fast frequency control schemes presented in Section 4. The converters of the test system are modelled as averaged two-level VSCs and have been implemented in MATLAB/Simulink. The MTDC system interconnects three separate ac grids to an OWF. The OWF and ac grid 3 (i.e. GSC3) export power into the dc grid. The OWF will also contribute to the fast frequency support via temporary overproduction (as discussed in Section 3). The parameters of the four-terminal system and the control gains of the frequency support schemes are summarised in Table 2. The ac grids are represented using simplified models with a base load capacity of 40 GW [29], [30]. The reader is referred to [7] for the complete parameters of the ac systems.

It should be highlighted that averaged models are employed instead of switching models since the studies performed in this paper do not require a detailed representation of the fast switching dynamics of power electronic converters. The adoption of averaged models also reduces the computational requirements [21].

6.1 Comparison of ACC, CC and DLC upgraded with the proposed ADC scheme

To demonstrate the performance of the proposed ADC scheme, two case studies are carried out. The fast frequency controllers are fitted with the proposed ADC scheme and with simulation results the effectiveness of the controls are compared with the ADC, without the ADC scheme and when no frequency control (NC) is considered.

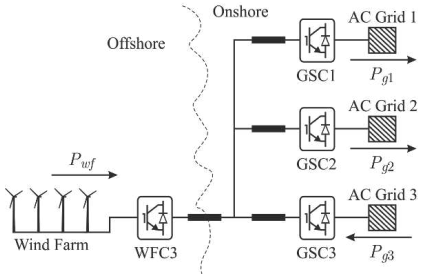

Figure 3: *Four-terminal VSC-HVDC test system.*

Table 2: *Parameters of VSCs and droop coefficients.*

Converter Parameters	
Power Rating	1000 MW
AC Voltage	380 kV
DC Voltage	±320 kV
DC Capacitor	223.26 μF
AC Inductor	11.35 mH
Supplementary Frequency Control Parameters	
k_{pv}	0.05 kV/MW
$k_{vp} = 1/k_{pv}$	20 MW/kV
k_{fv}	65 kV/Hz
$k_{fp} = k_{fv}/k_{pv}$	1300 MW/Hz
k_{off}	0.025 Hz/kV

6.1.1 *Case 1 - Single Imbalance:* Fig. 4 shows the results due to a generation loss of 1800 MW in Grid 2 at $t = 5$ s. With NC, there is no frequency support from the MTDC grid and the frequency in Grid 2 falls to 49.49 Hz (*i.e.* the frequency deviation is 0.51 Hz). When the ACC is in operation only, the responding ac systems (Grids 1 and 3) transferring additional power to the disturbed Grid 2 experience a drop of frequency (see Fig. 4). When the frequency drop exceeds $\Delta f_{db1} = 0.02$ Hz, the VSCs connected to Grids 1 and 3 enter the frequency sensitive mode. The dc voltage droop on all onshore converters is disabled and the dc grid voltage becomes unstable at $t = 8$ s (see solid red line in Fig. 4). This loss in control of dc voltage impacts the OWF active power as well because of the presence of the V_{dc}-f droop. It should be highlighted that the issues here highlighted are still present without an OWF providing fast frequency support [19].

With the proposed ADC present (denoted ACC+ADC), the converters connected to Grids 1 and 3 discriminate the frequency drop due to the provision of fast frequency support and change the set point from $\Delta f_{db1} = 0.02$ Hz to $\Delta f_{db2} = 0.1$ Hz. This operation prevents the VSCs connected to responding Grids 1 and 3 from entering the frequency sensitive mode. With the ADC fitted, the dc voltage remains stable while fast frequency support is provided (see solid blue line in dc voltage graph in Fig. 4). Also, unlike the case without ADC, the frequencies of Grids 1 and 3 return to their nominal values. This is a result of an increase in the powers of Grids 1 and 3 to their original values prior to the generation loss. As it can be observed, the frequency drop has been reduced to 0.39 Hz when the ACC scheme is used.

Fig. 5 shows the simulation results when the CC is employed, when the CC is upgraded with the ADC (denoted

CC+ADC) and when no corrective actions are taken (NC). When the CC is employed only, the VSCs connected to responding Grids 1 and 3 activate their frequency support mode and disable the active power-dc voltage droop. This results in a rapid drop of power injected into Grid 2 (see solid red line in GSC2 power in Fig. 5) and a further frequency drop on the disturbed grid at $t = 10$ s (see solid red line). With CC operating alone, there are unexpected power flows because of a maloperation or lack of coordination between the converters. For the case of CC+ADC, the sudden drop of power transferred to the disturbed Grid 2 is avoided by modifying the set-point of the dead bands on GSCs 1 and 3 from $\Delta f_{db1} = 0.02$ Hz to $\Delta f_{db2} = 0.1$ Hz. As it can be observed, there is an additional frequency drop at $t = 14$ s but this is due to the recovery period of the wind turbine.

A comparison is also made when all converters use the DLC scheme only, when DLC is used with the proposed ADC (denoted DLC+ADC) and without a supplementary frequency control (NC). Fig. 6 shows the simulation results. It can be observed that the DLC scheme employed on its own still maintains system stability and steady power flows. This occurs as the system has both power-voltage and frequency-voltage droops active in the disturbed operation. Given that the ADC delays the converters from switching to their frequency sensitive mode where the voltage droop is disabled, the ADC-upgraded DLC gives the same results as when the DLC is employed only. In other words, the ADC does not provide any benefits as with the DLC a voltage droop is always active both in normal and disturbed operation.

Table 3: *Frequency control schemes during single imbalance.*

	NC	ACC	CC	DLC	ACC+ ADC	CC+ ADC	DLC +ADC
Δf (Hz)	0.51	0.39	0.33	0.41	0.39	0.33	0.41
RoCoF (Hz/s)	0.18	0.156	0.15	0.159	0.156	0.15	0.159
Stable?	Yes	No	Yes	Yes	Yes	Yes	Yes

A comparison of the performance of the different frequency control schemes upon the single imbalance scenario is provided in Table 3.

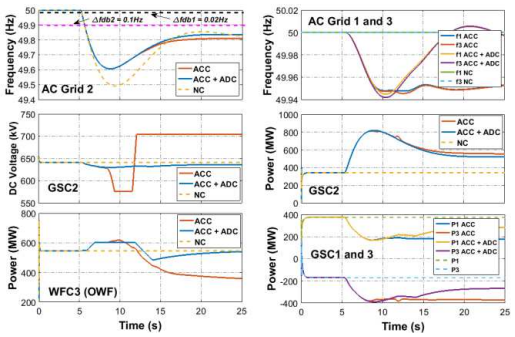

Figure 4: *Case 1, ACC scheme. System response after a generation loss of 1800 MW in Grid 2.*

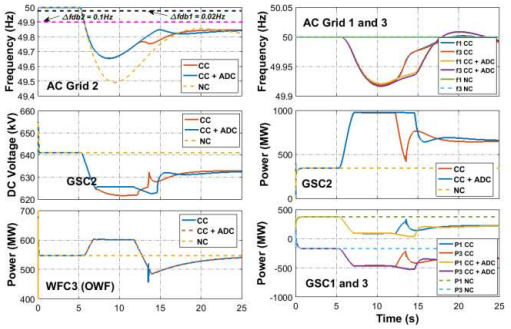

Figure 5: *Case 1, CC scheme. System response after a generation loss of 1800 MW in Grid 2.*

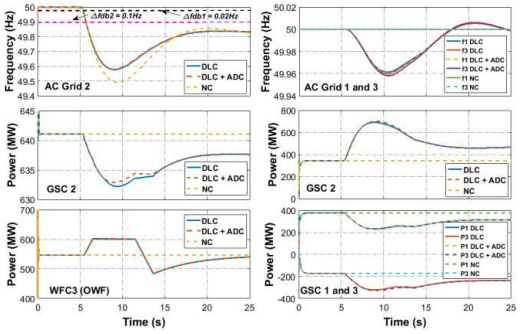

Figure 6: *Case 1, DLC scheme. System response after a generation loss of 1800 MW in Grid 2.*

6.1.2 *Case 2 - Opposing Frequency Trends:* The performance of the control schemes is demonstrated in this section during opposing frequency events (i.e. simultaneous loss of demand and generation). Simulations are performed when a generation loss of 1800 MW occurs in Grid 2 while a simultaneous demand loss of 900 MW occurs in Grid 3 at $t = 5$ s. The probability of these events occurring simultaneously in reality is low and, in any case, they may occur a few seconds after each other. However, having them occur simultaneously in simulations helps to stress the system and, this way, assess the capabilities of the proposed ADC scheme.

A comparison is made when all onshore converters use the ACC scheme only, when the ACC is upgraded with an ADC (ACC+ADC) and when no action is taken (NC), with results shown in Fig. 7. When the ACC is used on its own, the dc voltage droop on the onshore converters is disabled when the frequency deviation exceeds $\Delta f_{db1} = 0.02$ Hz. A sudden drop of dc voltage occurs around $t = 10$ s (see blue line on Fig. 7) due to only the *f-P* droop operating on GSCs 1, 2 and 3 and no converter controlling the dc voltage. This is also seen to affect the power from the OWF. When the ADC scheme is included, GSC1 modifies its set-point from $\Delta f_{db1} = 0.02$ Hz to $\Delta f_{db2} = 0.1$ Hz. Therefore, GSC1 retains control of the dc voltage using a V_{dc}-*P* droop and restores the dc grid operation during the provision of fast frequency support (see red line on Fig. 7).

Fig. 8 shows simulation results when the CC is used on its own, when the CC is upgraded with an ADC (CC+ADC) and with no frequency control (NC). When CC is used only, all

VSCs initiate the fast frequency controls, disable their P-V_{dc} droop and enable their f-V_{dc} droops. Therefore, no converter regulates active power in the MTDC grid. There are frequency oscillations in the ac grids as a result of power oscillations from the GSCs (see blue lines in Fig. 8). Also, as a result of these frequency oscillations, the OWF temporary overproduction translates the dc voltage change at $t \approx 12.5$s as a command to provide extra power again. For the case of CC+ADC, the ADC scheme allows the GSC1 to modify its set-point from $\Delta f_{db1} = 0.02$ Hz to $\Delta f_{db2} = 0.1$ Hz. As a result, operation of the power-voltage droop in GSC1 is maintained. This enables continuous stable dc voltage control, active power flow and frequency stability to the MTDC system (see solid red line in Fig. 8).

Fig. 9 shows the simulation results when DLC is used on its own, when used with the ADC (DLC+ADC) and with no frequency control (NC). As in Case 1, the DLC gives the same frequency response with and without the ADC, with power flow and dc voltage remaining stable.

A comparison of the performance of the different frequency control schemes upon the opposing frequency events is provided in Table 4.

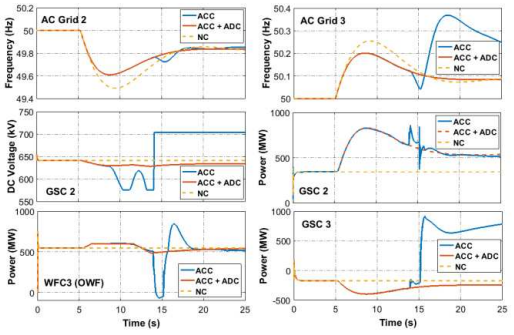

Figure 7: *Case 2, ACC scheme. System response after a generation loss of 1800 MW in Grid 2 and 900 MW demand loss at Grid 3.*

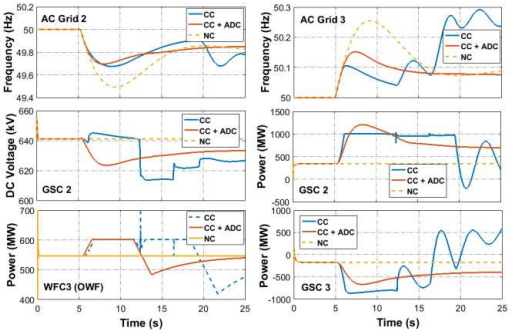

Figure 8: *Case 2, CC scheme. System response after a generation loss of 1800 MW in Grid 2 and 900 MW demand loss at Grid 3.*

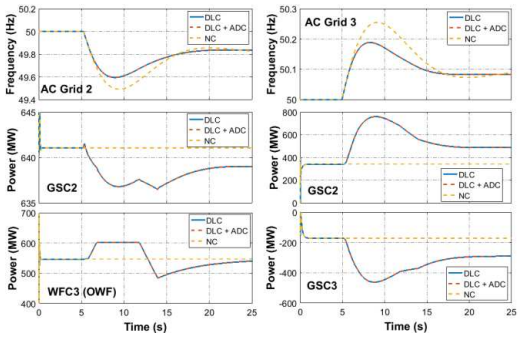

Figure 9: *Case 2. DLC scheme. System response after a generation loss of 1800 MW in Grid 2 and 900 MW demand loss at Grid 3.*

Table 4: *Comparison of support schemes during multiple imbalance*

	ACC	CC	DLC	NC	ACC+ ADC	CC+ ADC	DLC +ADC
Multiple Imbalance (Opposing Frequency Trend)							
Δf (Hz)	0.39	0.35	0.41	0.51	0.39	0.33	0.41
RoCoF (Hz/s)	0.156	0.143	0.159	0.18	0.156	0.141	0.159
Stable?	No	Yes	Yes	Yes	Yes	Yes	Yes

6.2 Fast Frequency Controllers with Proposed ADC Scheme

In this section, all schemes (CC, ACC and DLC) are upgraded with the proposed ADC and their effectiveness is compared when multiple grid disturbances occur (a generation loss of 1800 MW in Grid 2 and a demand loss of 900 MW in Grid 3 at $t = 2$ s). Simulation results are shown in Fig. 10 for the case of DLC+ADC, CC+ADC, ACC+ADC and when no corrective action is taken (NC).

An improved ac grid frequency deviation and *RoCoF* are achieved in all three schemes. The CC+ADC scheme (solid blue line) provides the most frequency support followed by the ACC+ADC scheme (solid red line). The DLC+ADC scheme provides the least frequency support because of its power-voltage and frequency-voltage droops operate simultaneously. However, this combined voltage and frequency droop operation in the DLC scheme allows for the continuous control of dc voltage during the provision of frequency support, therefore the DLC does not need the ADC to ensure stability. A droop correction factor has been suggested to overcome the limited support capability of the DLC, but this requires fast communications [16].

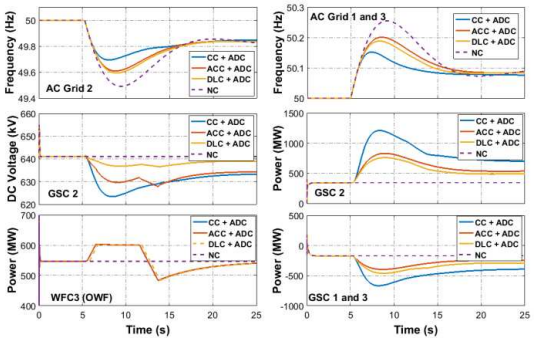

Figure 10: *Comparison of all schemes. System response after a generation loss of 1800 MW in Grid 2 and 900 MW demand loss at Grid 3.*

6.3 DC Grids with Different Frequency Control Modes

An additional study was carried out to investigate MTDC frequency support when each onshore VSC operates with a different frequency control scheme. Table 5 shows the supplementary control strategy used for each converter.

Fig. 11 shows simulation results due to a generation loss of 1800 MW in Grid 2 at $t = 5$ s. To show the benefits of the proposed ADC scheme, the performance is compared to the case when CC is employed only in GSC1 and ACC only in GSC2 and GSC3 (without ADC support). When the ADC is included, a stable dc voltage can be observed (see red line on Fig. 11(c)) as opposed to the case when CC and ACC are used on their own (see blue line on Fig. 11(c)). The proposed ADC scheme avoids a sudden or unwanted drop of power transferred through GSC1 and GSC3 (see Figs. 11(e)-(f)).

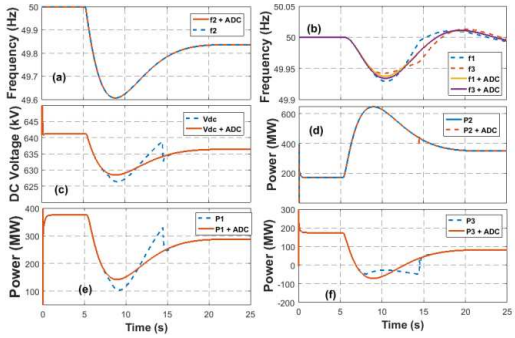

Figure 11: *Effect of the ADC scheme on different control modes in an MTDC system. Frequency variations in: (a) Grid 2; (b) Grids 1 and 3. (c) DC voltage variation. Power injections in: (d) GSC 2; (e) Grid 1; (f) Grid 3.*

Table 5: *Proposed system with different control modes*

Converter	Supplementary Frequency Control
GSC1	CC +ADC
GSC2	ACC +ADC
GSC3	ACC+ADC
WFC3	V_{dc}-f

7 Small-Signal Stability Study

To ensure that the supplementary frequency controls do not negatively affect the stability of the system, the small-signal model of the MTDC grid combined with the CC scheme for fast frequency support is derived. The CC scheme is selected for mathematical modelling because it was the most effective scheme when fitted with the ADC as shown by the results in Fig. 10. It produced the least frequency deviation and *RoCoF* compared to the other fast frequency schemes considered in this paper. The small-signal analysis shows the effect of the fast frequency control on the system modes and damping.

The combined MTDC grid including the fast frequency controllers can be described by the following state equation:

$$\dot{\mathbf{x}} = \mathbf{A}\Delta\mathbf{x} \quad (5)$$

where $\mathbf{x}$ is a vector denoting the states of the system. The stability of the system is determined by the eigenvalues of system matrix $\mathbf{A}$. The system is of 28th order. For mathematical modelling of the HVDC system the reader is referred to [31]. The ac grid is modelled according to [30] and the dc cables of both models are represented by resistors and inductors with parameters provided in [7].

To assess the validity of the small-signal model described by (5), this has been implemented in Simulink. Results from this model are compared with those obtained with the detailed model used in Section 6. System stability is assessed by calculation of the eigenvalues of system (5).

Figs. 12(a) and 12(b) show a comparison of the time-domain responses obtained with the small-signal and averaged models for a 10% step increase in power from the OWF. As it can be observed, the power variations in the different ac grids are similar for both models. With regards to dc voltage, it can be observed that the averaged model presents a faster response than its small-signal counterpart. The reason for this behaviour is due to the converters' inner control loops being modelled only in the small-signal model. However, it can be concluded that the overall dynamic performance agrees on well.

Fig. 13 shows the eigenvalues of the system for parametric variations in droop gains k_{fv} and k_{pv}. As it can be observed in Fig. 13(a), variations of k_{fv} from 30 to 65 kV/Hz do not affect the system eigenvalues (a close-up to the dominant eigenvalues is provided with the right-hand side plot); in other words, a variation in the frequency dead-band does not have an adverse effect in small-signal stability. Conversely, Fig. 13(b) shows the location of the eigenvalues as a function of droop constant k_{pv} in Grid 3, which has been modified from 0.005 to 0.15 MW/kV (i.e. from 10 to 300% of the original value). As it can be seen, the eigenvalues tend to exhibit a higher damping as k_{pv} increases. These results confirm that the system remains stable for a range of droop constants and, moreover, the frequency support schemes do not affect the normal operation of a system with proportional droop control.

8 Conclusions

In this paper, the effectiveness of three different fast frequency support schemes embedded in the terminals of MTDC grids has been assessed. As examined in this work, an unstable dc grid operation and reduced power transfer result from frequency variations on different ac systems connected to the dc grid during the provision of frequency support. This

also affects the capability of an OWF in providing synthetic inertia support.

To address these issues, an ADC scheme has been proposed and fitted to the frequency support schemes. It has been shown through simulations performed in MATLAB/Simulink that the inclusion of the ADC helps to restore a stable operation and to improve active power transfer during multiple frequency oscillations on the interconnected ac grids. The ADC scheme allows each VSC to discriminate the location of a frequency disturbance and to modify the dead-band set-point of its own local frequency control algorithm. Among the studied strategies, the CC scheme when upgraded with the ADC achieved the best performance, followed by the ACC scheme fitted with the ADC and then by the DLC scheme. It should be emphasised that the DLC may not need the ADC as its voltage droop is always active.

The small-signal stability study of the entire system with the CC scheme fitted to the converters was also carried out and compared against time domain simulations to validate the model and confirm system stability. It is shown that the frequency droop and dead-band do not affect the small-signal stability of the studied system. Results show that the ADC improves the coordination of frequency support of the MTDC system and the OWF.

9 Acknowledgments

The authors gratefully acknowledge the financial support from RCUK-EPSRC and National Grid under the project EP/L021455/1 “Impact of Low-Inertia and Low Short Circuit Levels on HVDC-rich AC grid” and by the EU FP7 Programme through the project “Beyond State of the art Technologies for re-Powering AC corridors & multi-Terminal HVDC Systems” (BEST PATHS), grant agreement number 612748.

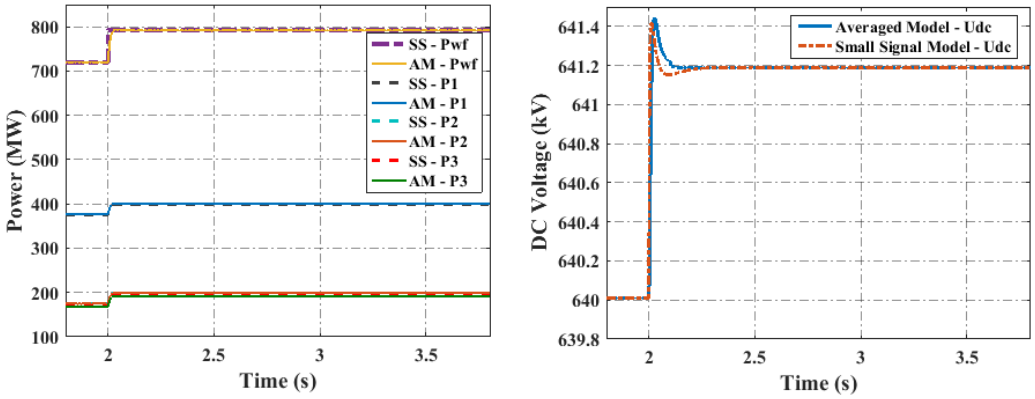

(*a*) (*b*)

Figure 12: *Response to 10% step increase in wind farm power output. Comparison of small signal model (SS) to averaged model (AM). (a) Power variation in OWF and Grids 1, 2 and 3. (b) DC voltage variation.*

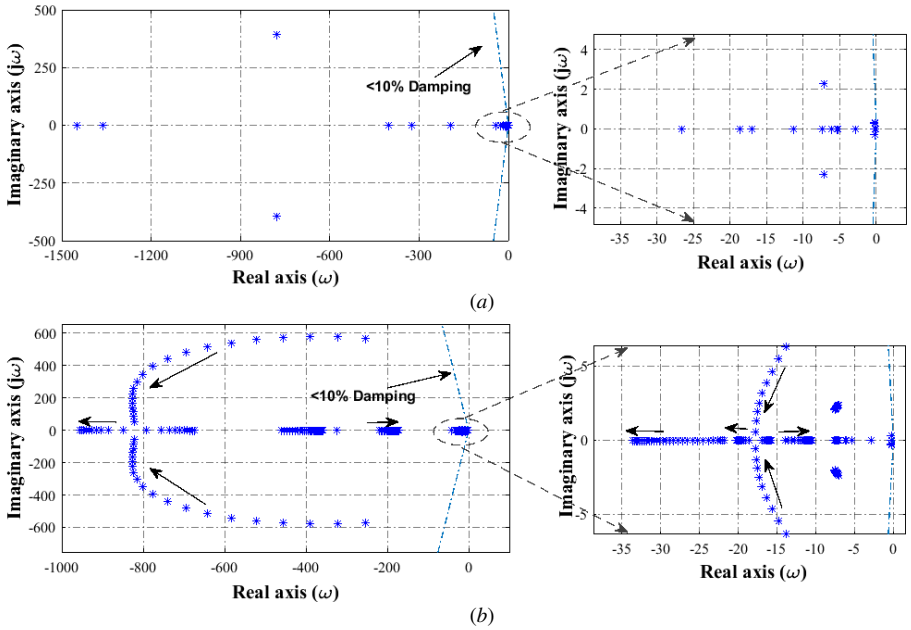

Figure 13: *Small-signal stability study of the system. (a) Root locus of the system for variations in droop gain k_{fv}. (b) Root locus of the system for variations in droop gain k_{pv}. In both cases, a zoomed view of the dominant eigenvalues is given by the right-hand side plots.*

10 References

[1] EWEA, "Wind energy scenarios for 2030," *EWEA*, 2015. [Online]. Available: https://www.ewea.org/fileadmin/files/library/publications/reports/EWEA-Wind-energy-scenarios-2030.pdf. [Accessed: 10-Dec-2017].

[2] National Grid, "Future Energy Scenarios: GB gas and electricity transmission," 2016. [Online]. Available: http://fes.nationalgrid.com/media/1292/2016-fes.pdf. [Accessed: 11-Apr-2018].

[3] L. Orellana, V. Matilla, S. Wang, O. D. Adeuyi, and C. E. Ugalde-Loo, "Fast Frequency Support Control in the GB Power System using VSC-HVDC Technology," in *7th IEEE International Conference on Innovative Smart Grid Technologies (ISGT Europe 2017)*, 2017, pp. 1–6.

[4] F. D. Bianchi, J. L. Domínguez-García, and O. Gomis-Bellmunt, "Control of multi-terminal HVDC networks towards wind power integration: A review," *Renew. Sustain. Energy Rev.*, vol. 55, pp. 1055–1068, 2016.

[5] B. Silva, C. L. Moreira, L. Seca, Y. Phulpin, and J. A. Pecas Lopes, "Provision of inertial and primary frequency control services using offshore multiterminal HVDC networks," *IEEE Trans. Sustain. Energy*, vol. 3, no. 4, pp. 800–808, 2012.

[6] P. Tielens and D. van Hertem, "Grid Inertia and Frequency Control in Power Systems with High Penetration of Renewables," in *Proceedings of the 6th IEEE Young Researchers Symposium in Electrical Power Engineering*, 2012, pp. 1–6.

[7] O. D. Adeuyi, M. Cheah-Mane, J. Liang, and N. Jenkins, "Fast Frequency Response from Offshore Multi-terminal VSC-HVDC Schemes," *IEEE Trans. Power Deliv.*, vol. 32, no. 6, pp. 2442–2452, 2017.

[8] F. Gonzalez-Longatt, E. Chikuni, and E. Rashayi, "Effects of the Synthetic Inertia from wind power on the total system inertia after a frequency disturbance," in *IEEE International Conference on Industrial Technology*, 2013, pp. 826–832.

[9] I. M. Sanz, B. Chaudhuri, and G. Strbac, "Inertial Response From Offshore Wind Farms Connected Through DC Grids," *IEEE Trans. Power Syst.*, vol. 30, no. 3, pp. 1518–1527, 2015.

[10] CIGRE Working Group B4.58, "Control methodologies for direct voltage and power flow in a meshed HVDC Grid," 2017.

[11] Y. Pipelzadeh, B. Chaudhuri, and T. C. Green, "Inertial response from remote offshore wind farms connected through VSC-HVDC links: A Communication-less scheme," *IEEE Power Energy Soc. Gen. Meet.*, pp. 1–6, 2012.

[12] J. N. Sakamuri, M. Altin, A. D. Hansen, and N. A. Cutululis, "Coordinated frequency control from offshore wind power plants connected to multi terminal DC system considering wind speed variation," *IET Renew. Power Gener.*, vol. 11, no. 8, pp. 1226–1236, 2017.

[13] Z. Miao, L. Fan, D. Osborn, and S. Yuvarajan, "Wind farms with HVdc delivery in inertial response and primary frequency control," *IEEE Trans. Energy Convers.*, vol. 25, no. 4, pp. 1171–1178, 2010.

[14] J. Rafferty, L. Xu, Y. Wang, G. Xu, and F. Alsokhiry, "Frequency support using multi-terminal HVDC systems based on DC voltage manipulation," *IET Renew. Power Gener.*, vol. 10, no. 9, pp. 1393–1401, 2016.

[15] L. Pan-Dian, Y. Zhi-Chang, C. Sheng, Z. Liang-He, and Y. Fen-Yan, "Review of Frequency Support Control Strategies for Asynchronous AC Systems Connected Through VSC-HVDC," in *2nd International Conference on Energy, Power and Electrical Engineering (EPEE 2017)*, 2017, pp. 414–421.

[16] S. Akkari, M. Petit, J. Dai, and X. Guillaud, "Interaction between the voltage-droop and the frequency-droop

control for multi-terminal HVDC systems," *IET Gener. Transm. Distrib.*, vol. 10, no. 6, pp. 1345–1352, 2016.

[17] T. Joseph, J. Gonçalves, C. E. Ugalde-Loo, and J. Liang, "Wind-Thermal Generation Coordination in Multi-Terminal HVDC-Connected AC Systems for Improved Frequency Support," in *13th IET International Conference on AC and DC Power Transmission (ACDC 2017)*, 2017.

[18] U. Tamrakar, D. Shrestha, M. Maharjan, B. Bhattarai, T. Hansen, and R. Tonkoski, "Virtual Inertia: Current Trends and Future Directions," *Appl. Sci.*, vol. 7, no. 654, pp. 1–29, 2017.

[19] K. Jose, O. Adeuyi, J. Liang, and C. E. Ugalde-loo, "Coordination of Fast Frequency Support from Multi-Terminal HVDC Grids," in *5th IEEE International Energy Conference (ENERGYCON 2018)*, 2018, pp. 1–6.

[20] J. Liang, T. Jing, O. Gomis-Bellmunt, J. Ekanayake, and N. Jenkins, "Operation and Control of Multiterminal HVDC Transmission for Offshore Wind Farms," *IEEE Trans. Power Deliv.*, vol. 26, no. 4, pp. 2596–2604, 2011.

[21] D. Van Hertem, O. Gomis-Bellmunt, and J. Liang, *HVDC Grids - For Offshore and Supergrid of the Future*, 1st ed. Wiley, 2016.

[22] J. Licari, C. E. Ugalde-Loo, J. B. Ekayanake, and N. Jenkins, "Damping of Torsional Vibrations in a Variable-Speed Wind Turbine," *IEEE Trans. Energy Convers.*, vol. 28, no. 1, pp. 172–180, 2013.

[23] K. F. Jose, O. D. Adeuyi, J. Liang, and C. E. Ugalde-Loo, "Inertial Contribution from Large Scale Variable-Speed Wind Turbines Connected to the GB Grid," in *13th IET International Conference on AC and DC Power Transmission (ACDC 2017)*, 2017.

[24] A. D. Hansen, M. Altin, I. D. Margaris, F. Iov, and G. C. Tarnowski, "Analysis of the short-term overproduction capability of variable speed wind turbines," *Renew. Energy*, vol. 68, pp. 326–336, 2014.

[25] M. Cheah-mane, "Frequency Response from DC grids," Barcelona, 2016.

[26] F. Díaz-González, M. Hau, A. Sumper, and O. Gomis-Bellmunt, "Participation of wind power plants in system frequency control: Review of grid code requirements and control methods," *Renew. Sustain. Energy Rev.*, vol. 34, pp. 551–564, 2014.

[27] National Grid, "System Operability Framework 2014," 2014. [Online]. Available: http://www2.nationalgrid.com/UK/Industry-information/Future-of-Energy/System-Operability-Framework/. [Accessed: 21-May-2015].

[28] K. Dallmer-Zerbe, E. Spahic, G. Kuhn, R. Morgenstern, and G. Beck, "Fast Frequency Response in UK Grid – Challenges and Solution," in *13th IET International Conference on AC and DC Power Transmission (ACDC 2017)*, 2017, pp. 1–6.

[29] Y. Mu, J. Wu, J. Ekanayake, N. Jenkins, and H. Jia, "Primary Frequency Response From Electric Vehicles in the Great Britain Power System," *IEEE Trans. Smart Grid*, vol. 4, no. 2, pp. 1142–1150, 2013.

[30] P. Kundur, *Power System Stability and Control*, Volume 7. New York: McGraw-Hill, 1994.

[31] G. Kalcon, G. Adam, O. Anaya-Lara, S. Lo, and K. Uhlen, "Small-Signal Stability Analysis of Multi-Terminal VSC-Based DC Transmission Systems," *IEEE Trans. Power Syst.*, vol. 27, no. 4, pp. 1818–1830, 2012.